Dynamical effects of inflation in ensemble-based data assimilation under the presence of model error

Article

Accepted Version

Dynamical effects of inflation in ensemble-based data assimilation under the presence of model error.

Scheffler Guillermo[1,2] | **Carrassi Alberto**[3,4] | **Ruiz Juan**[1,2] | **Pulido Manuel**[5,6,2]

[1]Centro de Investigaciones del Mar y la Atmósfera, CONICET-UBA, Departamento de Ciencias de la Atmósfera y los Océanos, FCEyN, UBA, Buenos Aires, Argentina

[2]UMI-IFAECI 3355 CNRS-CONICET-UBA, Buenos Aires, Argentina

[3]Dept. of Meteorology and National Centre for Earth Observations, University of Reading, UK

[4]Dipartimento di Fisica e Astronomia "Augusto Righi", University of Bologna, Italy

[5]Departamento de Física, FaCENA, UNNE, Corrientes, Argentina

[6]CONICET, Corrientes, Argentina

Correspondence
Scheffler Guillermo, Centro de Investigaciones del Mar y la Atmósfera, CONICET-UBA, Departamento de Ciencias de la Atmósfera y los Océanos, FCEyN, UBA, Buenos Aires, C1428EGA, Argentina
Email: guillermo.scheffler@cima.fcen.uba.ar

Funding information
Agencia Nacional de Promoción Científica y Tecnológica, PICT: 2033/2017 and University of Buenos Aires 20020170100504BA

Covariance inflation is one of the necessary tools enabling the success of ensemble Kalman filters (EnKFs) in high dimensional spaces and in the presence of model error. Inflation maintains the ensemble variance to a sufficiently large value, counteracting the variance damping at analysis times and its underestimate arising from model and sampling errors. In this work we investigate the effect of inflation on the dynamics of the EnKF ensemble. When the focus is on the recursive full cycle forecast-analysis-forecast, an apparently counter-intuitive effect of the multiplicative inflation appears in the span of the ensemble in the EnK. In particular, we demostrate that multiplicative inflation changes the alignment of ensemble anomalies onto the weakly-stable backward Lyapunov vectors. Whereas the ensemble is expected to collapse onto the subspace corresponding to the unstable portions of the Lyapunov spectrum, the use of multiplicative inflation contributes to retain anomalies beyond that subspace. Given that the presence of model error implies that the analysis error is no longer fully confined on the local unstable subspace, this feature of multiplicative inflation is of paramount importance for an optimal filtering. We propose hybrid schemes whereby additive perturbations complement multiplicative inflation by suitably

This article has been accepted for publication and undergone full peer review but has not been through the copyediting, typesetting, pagination and proofreading process which may lead to differences between this version and the Version of Record. Please cite this article as doi: 10.1002/qj.4307

increasing the dimension of the subspace spanned by the ensemble. The use of hybrid schemes improves analysis RMSE on the Lorenz 96 model compared to the use of multiplicative inflation alone, emphasizing the role of model dynamics when designing additive inflation schemes.

KEYWORDS
EnKF, Lyapunov, Model Errors, Multiplicative Covariance Inflation

1 | INTRODUCTION

Dynamical properties of forecast models play a key role on the performance of data assimilation (DA). For deterministic dynamics in a perfect-model scenario with linear dynamical and observational models, the span of the forecast error covariances of the Kalman filter (KF) and smoother (KS) aligns asymptotically with the subspace spanned by the backward Lyapunov vectors (BLVs) associated to non-negative Lyapunov exponents (Gurumoorthy et al., 2017; Bocquet et al., 2017; Bocquet and Carrassi, 2017). The connections between the filter/smoother error covariance and the underlying model Lyapunov spectrum have also been numerically established for the deterministic versions of the ensemble Kalman filter (EnKF) and smoother (EnKS), whenever the error regime is bound to be weakly nonlinear under the same deterministic and perfect model scenario (Bocquet and Carrassi, 2017). As a direct consequence, the minimal effective number of ensemble members required in an EnKF to achieve optimal performance is equal to the number of non-negative Lyapunov exponents (LEs). These findings extend to dynamical systems displaying a degeneracy in the spectrum of LEs, but with some caveats. In some coupled ocean-atmosphere models, the coupling manifests itself by the appearance of a quasi-flat portion of the LE spectrum with many LEs very close (within machine accuracy) to zero (Tondeur et al., 2020). In this case, the error covariance in a strongly coupled EnKF asymptotically aligns with the subspace spanned by the BLVs associated to all unstable plus all of the quasi-neutral modes, and the effective number of ensemble members must include all of those additional (possibly asymptotically stable) quasi-neutral LEs (Carrassi et al., 2022). The DA framework known as assimilation in the unstable subspace (AUS) exploits these features explicitly for the design of a DA methodology. In AUS the analysis solution is confined to the subspace spanned by the unstable and neutral BLVs (see e.g. Palatella et al., 2013 and references therein).

In the presence of random model errors the role of model dynamics on filter behavior and performance is less evident. In unstable stochastic linear systems with Gaussian errors, Grudzien et al. (2018a) proved that, because of the injection of random model error on all of the model degrees of freedom, the error projection onto stable BLVs is no longer dampened asymptotically to zero, even though it remains bounded. Nevertheless, the size of those bounds, which depends not only on the amplitude and rank of the model error covariance matrix but also on the variability of the local LEs (LLEs), can be too large. The mechanism is driven by events in which an asymptotically stable mode (with LLE < 0) experiences instantaneous error growth, thus the amplitude and frequency of these local bursts of instabilities impact on the bounds. Naturally, the weakly stable modes (those having an asymptotic LE ≈ 0) are the most relevant as their chances to be instantaneously unstable are larger. Unlike the deterministic system case, this behaviour implies the need to increase the effective number of ensemble members in an EnKF to include as many additional members as the number of weakly stable modes of high variability (Grudzien et al., 2018b).

Nevertheless, the increase of ensemble members only amounts to a necessary condition and it does not guarantee filter convergence. Local bursts of instability on the weakly stable modes contribute to enhance the so called *upwelling*

phenomenon (Grudzien et al., 2018b). That is, errors in the unfiltered subspace are upwelled to the filtered subspace in a reduced-rank filter, even if the unfiltered subspace only contains asymptotically stable directions. The effect is inherent to the reduced-rank formulation, thus it is present in deterministic systems, but it is much more pronounced in the presence of stochastic model errors. The upwelling mechanism provides a rationale and justifies the use of *covariance inflation* (see, *e.g.* Whitaker and Hamill, 2012) to counteract the filter underestimation of the actual forecast covariance caused by both sampling and model errors.

Covariance inflation is commonly applied under two forms: *multiplicative* and *additive*. *Multiplicative inflation* involves re-scaling the ensemble anomalies (*i.e.*, their deviations from the mean) by a scalar factor (Anderson and Anderson, 1999). Alternatively, *additive inflation* consists on adding random noise to each ensemble member (Hamill and Whitaker, 2005). Whitaker and Hamill (2012) suggest that multiplicative inflation methods may be more suitable for the treatment of sampling errors associated to the observation network density, whereas additive inflation can alleviate systematic model errors. In both cases, one has to tune the key parameters (*e.g.*, the amplitude of the rescaling factor in the multiplicative case and the amplitude of the noise in the additive case). This is a very costly procedure in high-dimensional spaces and not exempt of inaccuracies. Adaptive inflation schemes attempt to estimate those parameters online as part of the DA process and usually rely on observation-based diagnoses (Li et al., 2009; Miyoshi, 2011) or on estimating maximum likelihood parameters for covariance scaling (Anderson, 2009; Zheng, 2009; El Gharamti, 2018). Different approaches to adaptively inflate covariance matrices are compared by El Gharamti et al. (2019) showing that the combination of multiple adaptive inflation schemes can target different sources of errors such as sampling errors and model deficiencies. A comprehensive review of adaptive covariance inflation schemes can be found in Raanes et al. (2019).

Nonetheless, covariance inflation schemes do not take into account model dynamics explicitly in their formulation, nor it is fully understood how the aforementioned connection between the underling model instabilities and the filter error description behaves in the presence of inflation schemes. This is particularly noteworthy for multiplicative inflation schemes. In its simpler form, multiplicative inflation consists of a scalar coefficient left multiplying the covariance matrix. This spatially invariant configuration of covariance inflation is expected to have a negligible impact on the analysis covariance matrix rank and span at the time of its application. Nevertheless, as we shall show later, its use in sequential DA which alternates a forecast-analysis-forecast cycle, produces changes in the forecast and analysis error covariance rank and span. In contrast, additive inflation schemes introduce by construction stochastic noise that effectively perturbs the dynamical evolution of the ensemble anomalies.

In this context, perturbations from additive inflation that lay within the stable subspace are expected to vanish asymptotically similarly to what happens to model noise. However, transient instabilities may drive additive perturbations onto the filtered (presumably unstable-neutral) subspace. This mechanism puts in evidence how the efficacy of additive inflation is affected by the underlying model instability properties. We shall show however that an interplay also exists, contrary to our original belief, for multiplicative inflation.

Our work aims at studying in depth the relation between nonlinear model dynamics and the functioning of the ensemble Kalman filter upon the presence of model error. In particular, the interplay between model instabilities and the inflation scheme. We demonstrate that, by the sole introduction of multiplicative covariance inflation, the EnKF may span a subspace beyond the most unstable directions. New inflation methods are proposed that focus on decomposing the ensemble anomalies to properly account for model errors upwelled from asymptotically stable modes. This is achieved by targeting inflation of ensemble anomalies based on their degree of alignment onto unstable or weakly stable BLVs respectively.

2 | PROBLEM AND EXPERIMENTAL SETTINGS

Let the state and observations be defined through a nonlinear state space model:

$$\mathbf{x}_k = \mathcal{M}_k(\mathbf{x}_{k-1}) + \boldsymbol{\eta}_k, \qquad k = 1, 2, \ldots \tag{1}$$

$$\mathbf{y}_k = \mathbf{H}\mathbf{x}_k + \boldsymbol{\nu}_k. \qquad k = 1, 2, \ldots \tag{2}$$

The state $\mathbf{x}_k \in \mathbf{R}^n$ evolves according to the nonlinear autonomous dynamical model $\mathcal{M}$ from time t_{k-1} to t_k. Observations $\mathbf{y}_k \in \mathbf{R}^p$ are related to the state through an observation operator matrix, $\mathbf{H} \in \mathbf{R}^{p\times n}$, assumed here, for the sake of simplicity, to be linear. The model error, $\boldsymbol{\eta}_k$, and the observational error $\boldsymbol{\nu}_k$ are assumed to be mutually independent and to be Gaussian distributed with zero-mean and covariance $\mathbf{Q}$ and $\mathbf{R}$ respectively. The filter performance is strongly dependent on the the filter's knowledge about $\mathbf{Q}$ and $\mathbf{R}$, and their estimation is a key challenge in ensemble Kalman filter (EnKF; Evensen et al. (2009)) methods and DA in general (Dee, 1995; Pulido et al., 2018; Tandeo et al., 2020). In this study, we assume that the correct $\mathbf{Q}$ and $\mathbf{R}$ are known by the filter and we can thus concentrate on studying the impact of model error and inflation on ensemble span. State estimation is performed using the ensemble transform Kalman filter (ETKF, Hunt et al., 2007; Bishop et al., 2001), that is a deterministic (square root) EnKF Tippett et al. (2003). As for all EnKFs the forecast error covariance is approximated using an ensemble of model trajectories. The ensemble members are evolved using the nonlinear dynamical model to obtain a forecast ensemble $\{\mathbf{x}_k^{\mathrm{f(i)}} \mid i = 1, 2, \ldots, N\}$:

$$\mathbf{x}_k^{\mathrm{f(i)}} = \mathcal{M}_k(\mathbf{x}_{k-1}^{\mathrm{a(i)}}), \qquad k = 1, 2, \ldots, \qquad i = 1, 2, \ldots, N \tag{3}$$

where $\mathbf{x}_k^{\mathrm{a(i)}}$ is the i-th member analysis state at the k-th assimilation cycle and N is the ensemble size.

We shall consider a trajectory generated by Eq. (1) as the "true state". Synthetic observations are generated with Eq. 2 and the hidden true state is then estimated from the set of noisy observations using the ETKF. The ensemble members are propagated in time using the deterministic model, Eq. (3) . This choice allows us to isolate the effect of the covariance inflation on the ensemble, without being directly contaminated by noise. At the same time, model error is present in our problem by perturbing the truth.

Experiments are performed using the Lorenz 96 model (Lorenz, 1996; Lorenz and Emanuel, 1998) with $n = 40$ variables and forcing $F = 8$. In this configuration the dynamical system contains $n_0 = 14$ non-negative LEs. The model is numerically integrated with a timestep, $\delta t = 0.05$, for $1,250$ model time units (*i.e.* for $25,000$ time steps). The state is completely observed, *i.e.* $p = n$, at every model time step, with an observational error covariance set to $\mathbf{R} = 0.05^2\mathbf{I}_n$. The choice of such an observational constraint is intentional, and it is required to maintain the evolution of the state estimation error within a linear or weakly nonlinear regime, such that the dynamics of the system could be reasonably modelled using the BLVs. BLVs are estimated at every model timestep using the orthonormalization process described in Legras and Vautard (1996).

The model error covariance is a scaled version of the covariance used by Grudzien et al. (2018b),

$$\mathbf{Q} \triangleq [Q]_{ij} = \begin{cases} 0.5\sigma_q^2 & \text{if } i = j \\ 0.25\sigma_q^2 & \text{if } i = j \pm 1 \\ 0.125\sigma_q^2 & \text{if } i = j \pm 2 \\ 0 & \text{otherwise,} \end{cases} \tag{4}$$

where $1 \leq i, j \leq n$ and $Q_{i,-j} = Q_{i,n-j}$ for $j < 1$. The experiments were conducted with an ensemble size of $N = 32$ members, with initial state drawn from the normal distribution, $\mathcal{N}(\mathbf{x}_0, \sigma_b^2 \mathbf{I}_n)$. After an initial exploratory analysis, we set $\sigma_b = 0.5$ but results were insensitive to the choice of σ_b after a spin-up period. A multiplicative inflation factor is applied to the ensemble-based forecast error covariance matrix before being used in the analysis. This factor is adaptively adjusted in time (while being uniform in space, i.e. a single global parameter) at each assimilation step using the adaptive multiplicative inflation scheme proposed in Miyoshi (2011). . In all of the experiments, the first 2,500 assimilation cycles are discarded from the diagnostics calculations. For the sake of robustness, all results are averaged over 10 repetitions of the assimilation experiments, each one using different initial ensemble and different observational error samples.

To properly understand dynamical properties of the ensemble in the perfect and imperfect model cases, we analyze the alignment of ensemble anomalies with the BLVs. Ensemble anomalies at time k are defined as $\mathbf{A}_k^{(i)} = \mathbf{x}_k^{\mathrm{a}(i)} - \overline{\mathbf{x}}_k^{\mathrm{a}}$ for each of the $i = 1 \ldots N$ ensemble members. Following Bocquet and Carrassi (2017) we define the mean angle between ensemble anomalies $\mathbf{A} \in \mathbb{R}^{n \times N}$ and the j-th BLV, stored as the j-th column of the matrix $\mathbf{E}_k^j$ at time t_k as

$$\theta_k^j = \frac{1}{N} \sum_{i=1}^{N} \theta_k^{i,j} = \frac{1}{N} \sum_{i=1}^{N} \arccos \left\{ \frac{(\mathbf{E}_k^j)^\top \mathbf{A}_k^{(i)}}{\|\mathbf{A}_k^{(i)}\|} \right\}, \tag{5}$$

with $\theta_k^j \in [0, \pi]$ and $1 \leq j \leq n$, and where $\mathbf{A}_k^{(i)}$ is the $i-th$ column of the anomaly matrix $\mathbf{A}$, such that $(N-1)\mathbf{P}^f = \mathbf{A}\mathbf{A}^\top$

A description of the assimilation cycle and BLVs computation is given in Algorithm 1.

In the first set of experiments, we compare the time averaged filter covariance matrix $\mathbf{P}^{\mathrm{a}}$ with an alternative estimate of the actual covariance matrix of analysis errors. The actual covariance of analysis errors is unknown in most applications but we use its structure as a baseline to evaluate the sample covariance resulting from the filter. The actual covariance is empirically approximated using the true analysis errors over multiple experiment repetitions, all with the same observations but different initial ensembles. The "actual" covariance is then approximated as $\mathbf{P}^{\mathrm{a}}_{\mathrm{true}}(t_k) = \boldsymbol{\varepsilon}_k^{a\top} \boldsymbol{\varepsilon}_k^a$, where $\boldsymbol{\varepsilon}_k^a = \overline{\mathbf{x}}_k^a - \mathbf{x}_k$ represents the analysis error at time k and $\overline{\mathbf{x}}_k^a$ is the analysis state at time k. We used 50 experiment repetitions to compute the "actual" error covariance matrix. In the next sections we drop temporal dependencies from covariance matrices to keep the notation simple, but note that dynamical properties such as projection angles and matrix rank are computed at each assimilation step and then averaged in time.

Algorithm 1 Assimilation cycle and calculation of anomaly projection

Given initial state $\mathbf{x}_0$ at time t_0
Initialize perturbations matrix $\mathbf{E}_0 = \mathbf{I}$ for BLVs calculation
for each timestep t_k in $k = 1 \dots T$ **do**
  Integrate true dynamical system $\mathbf{x}_k = \mathcal{M}_k(\mathbf{x}_{k-1}) + \boldsymbol{\eta}(k)$
  Compute the Jacobian $\mathbf{J}_{k-1}$ by linearizing at $\mathbf{x}_{k-1}$
  Evolve perturbations linearly $\rightarrow \tilde{\mathbf{J}}_k = \mathbf{J}_{k-1}\mathbf{E}_{k-1}$
  Determine BLV $\mathbf{E}_k$ by applying QR-decomposition on the perturbations $\rightarrow \mathbf{E}_k\mathbf{R}_k = \tilde{\mathbf{J}}_k$
end for
Gather observations $\mathbf{y}_k$ at times t_k for $k = 0 \dots T$
Initialize ensemble $\mathbf{X}_0^f \in \mathbb{R}^{n\times N}$ with size N at time $t = 0$ ($N = 32$ in our experiments)
for each timestep t_k in $k = 1 \dots T$ **do**
  Integrate forward the ensemble and get $\mathbf{x}_k^f = \mathcal{M}_k(\mathbf{x}_{k-1}^f)$
  Compute the global inflation parameter at t_k, $\alpha_k = \alpha_k(\mathbf{X}_k^f, \mathbf{y}_k)$
  Compute the analysis ensemble with the ETKF, $\mathbf{x}_k^a = \mathrm{ETKF}(\mathbf{x}_k^f, \mathbf{y}_k, \alpha_k)$
  Compute analysis ensemble mean $\overline{\mathbf{x}}_k^a = \frac{1}{N}\sum_j \mathbf{x}_k^{a(j)}$
  Compute the average angle θ_k between each of the analysis ensemble anomalies and $\mathbf{E}_k$ using Eq. 5
end for
Calculate time and ensemble averaged angle $\overline{\theta}$

3 | ENSEMBLE AND UNSTABLE SUBSPACES WITH MODEL ERROR AND THE ROLE OF MULTIPLICATIVE INFLATION

3.1 | The role of model error

To gain insight on the role of model error, we run first a set of experiments using a perfect model scenario (*i.e.* $\mathbf{Q} = 0$) that will serve as benchmark. Figure 1a (purple line) shows that the eigenvalues of the analysis error covariance matrix $\mathbf{P}^a$ vanish beyond the rank $r > n_0 = 14$. This confirms the asymptotic alignment of the ensemble subspace with the unstable-neutral subspace. This result is in agreement with that in Bocquet and Carrassi (2017) even though a different deterministic square-root EnKF (see *e.g.* Tippett et al., 2003; Bocquet et al., 2015) is used in that work. The incorporation of additive model error (blue and yellow lines) results in a flattening of the eigenspectrum of $\mathbf{P}^a$ and it is no longer bounded to the first 14 eigenvalues. .

The spectrum of eigenvalues of $\mathbf{P}^a_{\text{true}}$ is shown in Fig. 1b. The true error covariance, $\mathbf{P}^a_{\text{true}}$, exhibits a flattening of the eigenspectrum as model error increases (*cf* blue and yellow lines in Fig. 1b), yet model error does not increase the rank of $\mathbf{P}^a_{\text{true}}$ as drastically as for the ensemble-based $\mathbf{P}^a$, suggesting that the actual analysis error is less sensitive to model error than as ensemble based covariance $\mathbf{P}^a$. We hereafter focus on ensemble based covariances $\mathbf{P}^a$.

The time averaged angle θ is shown in Fig. 1c. In the perfect model case (purple line), we see a clear cut-off in the projections around rank $n_0 = 14$, marking the net difference between the stable and the unstable-neutral portions of the Lyapunov spectrum. The ensemble anomalies have negligible projections onto the stable subspace. Cut-offs are visible in the experiments with model error too, but they occur now in correspondence to larger BLV ranks directly proportional to the size of the model error (*i.e.*, the larger the model error the higher the rank). The projection of $\mathbf{P}^a$ onto the stable subspace no longer vanishes under this model settings, a behaviour consistent with what was anticipated by Grudzien et al. (2018a) for linear systems. Figure 1c reveals also that the emergence of anomalies in

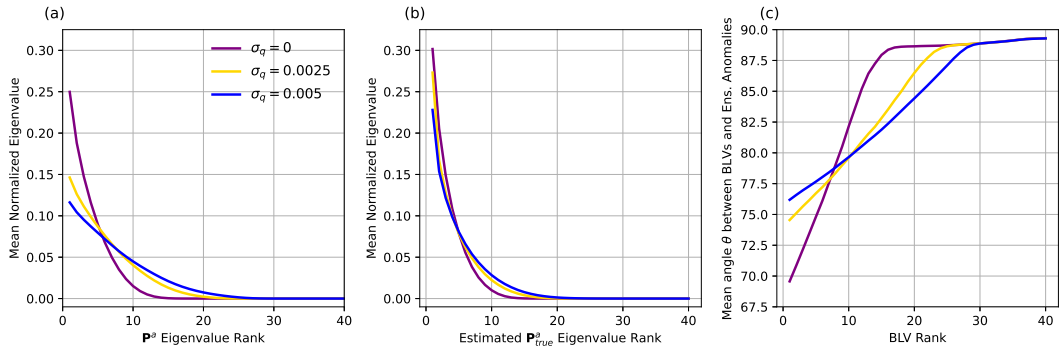

FIGURE 1 (a): Normalized mean eigenvalues of the ETKF analysis error covariance matrix $\mathbf{P}^a$ for different model error amplitudes $\sigma_q = (0; 0.0025; 0.005)$. Background covariances were artificially inflated using a multiplicative adaptive covariance scheme (Miyoshi, 2011). (b): Normalized mean eigenvalues of the covariance of analysis errors $\epsilon^a_k = \mathbf{x}_k - \overline{\mathbf{x}}_k$ calculated over 50 repetitions with same assimilation set up as (a). (c): Time and ensemble averaged angle θ of ensemble anomalies onto the backward Lyapunov vectors (BLVs). Multiplicative adaptive inflation coefficients averaged over time were $(1.01; 1.114; 1.182)$ respectively.

weakly-stable directions is counterbalanced by a reduction in the projection onto leading BLVs ($r \leq 7$). This effect is reminiscent of the role of growing nonlinearities in a perfect model setting as described by Bocquet and Carrassi (2017).

Figure 2 shows projections of forecast and analysis ensemble anomalies onto BLVs, for two observational scenarios, dense and sparse experiments. The "dense" case refers to our main experimental setup with the system fully observed at each time step. Recall that this scenario is intentionally used to maintain the error evolution linear or weakly-nonlinear, such that the unstable-neutral subspace spanned by the BLVs can be a proxy of the ensemble span. This choice is common (see *e.g.*, Carrassi et al. (2022)) and a discussion on how to modulate the observational constraint to efficiently achieve quasi linear error evolution is given in Bocquet et al. (2017). In the "sparse" experiment the system is observed at every other state variable and observation interval is increased to 5 timesteps. For both experiments we show results for the analysis and forecast error covariance matrices. In the presence of a dense observational network, the subspace spanned by the forecast and analysis error is confined within as many BLVs as $r <= 27$. The forecast and analysis projections are, in this case, very similar to each other with the error subspaces showing a linear decrease in projections onto BLVs of growing rank.

The situation changes in the sparse experiment. Here, a reduction of the ensemble span dimension to $r = 20$ is found and the alignment with the leading 10 BLVs is more acute with a mean angle similar in magnitude to the case without model errors (*cf* purple line in Fig. 1c) for both analysis and forecast anomalies. We argue that this is primarily due to the increased observational interval: error growth driven by the dynamical instabilities dominates the forecast error, proportionally more than the model errors. The latter still affects the forecast error, otherwise it will be strictly confined within the unstable-neutral subspace, yet the model role is smaller than in the dense experiment. A larger forecast error also implies a larger assimilation increment, resulting in the analysis error span deviating more from the forecast error span, than it does in the dense case. The angle between the projection of analysis anomalies and BLVs (blue line in Fig. 2) confirms this discrepancies and suggests that model error drives analysis error covariance to align with higher order BLVs. We see however the same linear profile of projections in the analysis error as before. In

the next subsection we will explore whether such a change in covariance structure is a direct consequence of model errors or an instrumental response to covariance inflation.

In what follows we shall focus on the spatially and temporally dense observation network scenario. Furthermore, in line with previous studies (see e.g. Bocquet and Carrassi, 2017; Grudzien et al., 2018a), we largely study the properties of the analysis error covariance matrix. Given the order of the semi-positive definite matrices we have $\text{rank}(\mathbf{P}^a) \leq \text{rank}(\mathbf{P}^f)$, the findings we describe for $\mathbf{P}^a$ should also hold for $\mathbf{P}^f$ on this experimental setup.

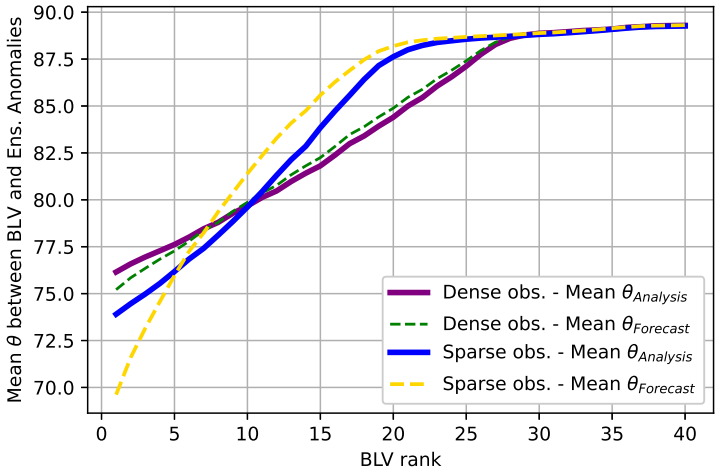

FIGURE 2 Time and ensemble averaged angle θ of forecast (traced lines) and analysis (solid lines) ensemble anomalies projected onto the backward Lyapunov vectors (BLVs) for model error $\sigma_q = 0.005$. Sparse observation network setup corresponds to a highly constrained observations scenario in which observations are available for every other variable and every 5 numerical timesteps.

3.2 | The role of inflation

We investigate now the impact of covariance inflation on the span and rank of the EnKF anomalies matrix, and on how these anomalies project onto the BLVs. The time-average multiplicative covariance inflation factors for the three experiments are reported in Table 1, together with the corresponding analysis RMSE . The inflation factor in the adaptative scheme by Miyoshi (2011) is calculated based on a Bayesian formulation. It is minimal in the perfect model case, and it increases proportionally with the degree of the model error.

In order to elucidate the possible interplay between inflation and the rank of the anomaly matrix anomalies matrix rank, we show in Fig. 3 the average number of eigenvalues explaining a portion of the full matrix variance (blue) as well as the analysis RMSE (red), both as a function of the (intentionally fixed, *i.e.* non adaptive) inflation factor, for perfect (left panel) and model error (right panel) case with $\sigma_q = 0.005$.

Figure 3 suggests that, contrary to our expectations, multiplicative inflation is effective in increasing the rank of the EnKF error covariance matrix. This does not imply that the filter performance improves. In fact, the RMSE in

TABLE 1 Analysis RMSE and time-average multiplicative adaptive inflation coefficient, α, for different levels of model error.

Model Error Amplitude	$\sigma_q = 0$	$\sigma_q = 0.0025$	$\sigma_q = 0.005$
Analysis RMSE	0.008	0.014	0.016
Time-mean inflation coefficient - α	1.01	1.114	1.182

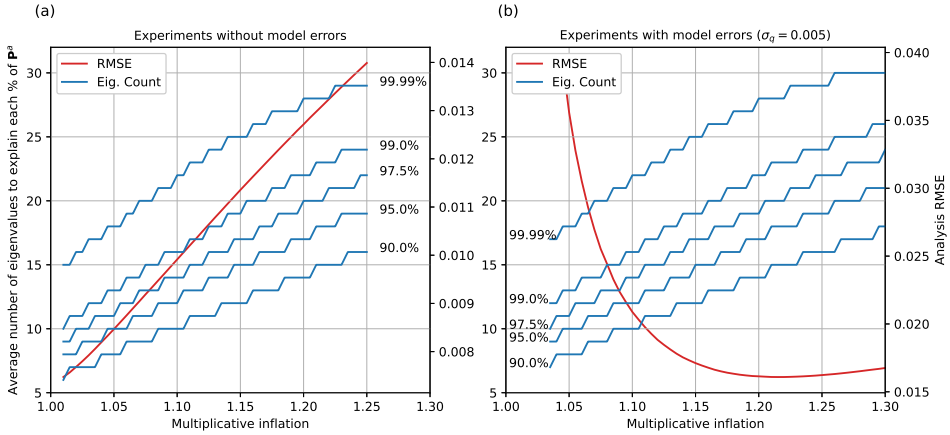

FIGURE 3 Average number of eigenvalues of $\mathbf{P}^a$ required to explain a portion of the full analysis error variance (blue) and the analysis RMSE (red) as a function of the fixed multiplicative covariance inflation. Results are shown for the perfect model case (a), and model error case with $\sigma_b = 0.005$ (b). Results are averaged over 15,000 assimilation cycles. Multiplicative inflation values α that are not large enough to avoid filter divergence were intentionally excluded.

the perfect model case grows monotonically when the inflation factor exceeds 1.01. Note from Table 1 that the time-averaged adaptive inflation factor is in this case about 1.01. Similarly, in the model error scenario, the RMSE grows after its minimum at 1.21, which is close to the time-averaged adaptive inflation (*cf* Table 1).

Multiplicative inflation consists in multiplying the ensemble-based forecast covariance matrix by a global scalar coefficient. Thus, how can multiplicative inflation change the covariance matrix's rank? Results in Fig. 3 shed light on an important dynamical property of multiplicative inflation. One would expect at first sight that multiplicative inflation, as opposed to additive inflation, preserves the span and rank of the analysis anomalies and only affects their amplitude during the analysis step. Nevertheless, even though the application of the multiplicative inflation at each individual analysis time does in fact leave unchanged the rank and span (it only amounts to a scalar coefficient multiplying the matrix), its recursive application produces a long-term effect of a different nature, altering the span of the covariance matrix. We conjecture this to be a direct consequence of the amplification of ensemble perturbations introduced by multiplicative inflation. Whereas one would expect that linear perturbations introduced during the analysis step would remain linear, those anomalies are pushed beyond the linear subspace by the nonlinear model during forecast step. Eventually, these residual errors would be dampened by model dynamics but in contrast they are amplified on every assimilation cycle by the application of inflation, and then upwelled to the filtered modes, according to the mechanism

described by Grudzien et al. (2018b). Such a behavior should be more pronounced in the presence of model error, not only due to the increased bursts of instability on the more stable directions, but also due to the required increase of multiplicative inflation. This is confirmed in Fig. 3 by observing that the minimum number of eigenvalues per each variance threshold and the required inflation factor are both larger in the case with model error than in the perfect model case (*cf* the blue curves in the two panels). It should be noted that the eigenvalue threshold is approximately the same for each inflation factor setting regardless of the presence of model errors. Therefore multiplicative inflation in sequential ensemble-based DA produces two effects: (i) it alleviates sampling error sub-estimation of the covariance and represents crudely model error in the filtered subspace and, (ii) it contributes to maintain the filtered subspace dimension to a high value. As shown in Fig. 3, the rank is as high as 27 in the model error experiment, in correspondence to an inflation factor of $\alpha \approx 1.21$.

Additional evidence for multiplicative inflation driving the changes in ensemble projections is provided in Fig. 4 by exploring whether the structure of ensemble anomalies depends directly on the changes induced by multiplicative inflation. Figure 4 shows the anomalies projected onto the BLVs for the perfect and imperfect ($\sigma_q = 0.005$) model scenarios. In each case, two types of experiments are performed with different multiplicative inflation factors. In the first experiments, the inflation is fixed to the value obtained by averaging the corresponding adaptive inflation values (*cf*, Table 1). They are $\alpha = 1.01$ and $\alpha = 1.18$ for the perfect and imperfect model case respectively. In the second set of experiments, the inflation is set to non optimal values, $\alpha = 1.18$ and $\alpha = 1.025$ (the latter is the minimum inflation value required to avoid filter divergence) respectively. Results indicate that changes in the alignment of ensemble anomalies onto BLVs are directly related to the amplitude of multiplicative inflation and not necessarily to the presence of model errors. We recall however that the experiments with non optimal inflation are done for the sake of studying the effect on the alignment of anomalies onto the BLVs, despite the associated RMSE being larger than in the optimal case.

Results shown in Fig. 4 confirm our conjecture on the role of multiplicative inflation: it causes changes in the span of the ensemble anomalies. By amplifying error representation outside the unstable-neutral subspace, the multiplicative inflation induces an increase of the ensemble span. This "artificial" rank increase does not necessarily imply reductions in the filter state estimation error (the RMSE is much larger than when the optimal or adaptive inflation is used in either case), but it nevertheless reveals of an unknown effect of multiplicative inflation.

3.3 | Reduced-rank model error within the unstable subspace

In all of the previous experiments, model error in the state space was full-rank, *i.e.* the model error realizations were sampled from a normal distribution with a full-rank covariance matrix $\mathbf{Q}$ given in Eq. (4). Model error is thus injected on all of the model variables, enhancing the upwelling of error from unfiltered to filtered directions as described in Grudzien et al. (2018b). We have also seen that multiplicative inflation prevents the full collapse of the ensemble to the neutral-unstable subspace.

In this section, we conduct another set of experiments inspecting the correspondence between the model error rank and EnKF $\mathbf{P}^{\mathrm{a}}$, in particular to corroborate whether the rank of $\mathbf{P}^{\mathrm{a}}$ would have also changed if model error only spans the unstable-neutral subspace. We devised a proof-of-concept experiment in which all of the model error instantaneous realizations are confined by construction within the subspace spanned by the BLVs associated with non-negative local Lyapunov exponents (LLEs). To achieve this, model error is sampled from $\mathcal{N}(0, \sigma_q \mathbf{L_k Q L}_k)$, where $\mathbf{L}_k = \mathbf{E}^{\mathcal{U}}\mathbf{E}^{\mathcal{U}\mathsf{T}}$ is the orthonormal projector constructed using the local unstable-neutral BLVs, the columns of $\mathbf{E}^i$, where $i = 1, ..., n_{0k}$ is used to identify that the number of non-negative LLEs fluctuates in time. After being sampled, the norm of model error realizations is rescaled to be consistent with that of the full rank $\mathbf{Q}$ experiments.

By confining the model error within the locally unstable-neutral subspace, the forecast error covariance is better

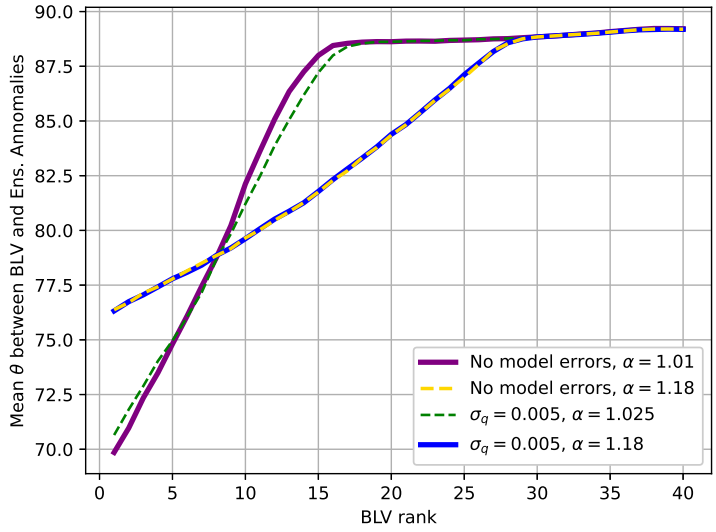

FIGURE 4 Time averaged angle θ (degrees) of the ensemble anomalies projected onto the BLVs for the perfect and imperfect ($\sigma_q = 0.005$) model scenarios and different fixed multiplicative inflation values (α). Results are averaged over 15,000 assimilation cycles.

approximated by the EnKF. This is reflected by a time average RMSE of 0.013 for the experiment with $\sigma_q = 0.005$ compared to 0.016 obtained in the full-rank case (*cf* Table 1): RMSE is even slightly below the case of smaller (but full rank) model error, *i.e.* $\sigma_q = 0.0025$. The time-averaged adaptive multiplicative inflation coefficient is also reduced from 1.18 to 1.13. The projection of the ensemble anomalies onto the BLVs (Fig. 5a) shows a great similarity with the former full-rank model error experiments (denoted by $\mathbf{Q}^{\text{full}}$). The current confined model error case is also shown in Fig. 5a (denoted by $\mathbf{Q}^{+\text{LLE}}$). Multiplicative inflation therefore increases the subspace spanned by the ensemble to new directions which are not directly spanned by model errors. Nevertheless a notable distinction is that the anomalies in the full-rank case have non-negligible projections on a few more BLVs. This is consistent with inflation factor being slightly larger in the full-rank case.

A further understanding of the filter dynamical properties is provided by looking at the mean angle between the analysis error and the BLVs defined as,

$$\gamma_k^j = \arccos\left\{\frac{(\mathbf{E}_k^j)^\top \boldsymbol{\varepsilon}_k^a}{\|\boldsymbol{\varepsilon}_k^a\|}\right\}. \tag{6}$$

In the perfect model case, the angle between the BLVs and the analysis error (Fig. 5b) and that with the ensemble anomalies (Fig. 5a) are almost identical, indicating a proper functioning of the EnKF, with the ensemble anomalies properly spanning the directions where the actual error is confined. When model error is incorporated, error projections span a broader subspace than anomalies. In the case of model error projecting only on unstable directions, the increased span of analysis errors could be associated to an increased degree of nonlinearity due to the presence

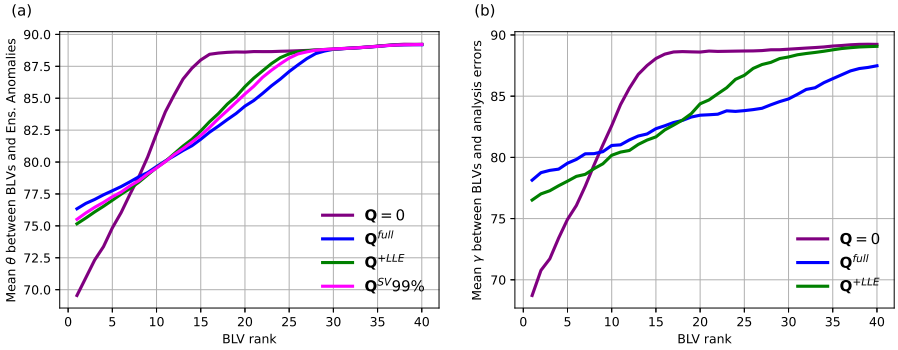

FIGURE 5 (a) Time averaged angle θ (degrees) between ensemble anomalies and the BLVs for different configurations of model error. (b) Time and ensemble averaged angle γ (degrees) of the analysis errors onto the backward Lyapunov vectors (BLVs) for different representations of model error. Namely, no model error (purple), full rank model error covariance (blue), and model error projected onto locally unstable BLVs (green), model error projected onto decomposed anomalies up to the singular value s_0 (pink).

of errors. In the case with full-rank model errors, the projections onto the BLVs of the anomalies differ significantly from those of the actual error, particularly in the more stable directions. This indicates in both model error scenarios that the subspace spanned by the ensemble anomalies is not sufficient to capture existing errors, in spite of their source. Error projections onto BLVs of rank 20 up to 25 are particularly noteworthy and it is clear that multiplicative inflation is only able to handle model errors on the leading and weakly stable directions. We note that whereas we have shown that multiplicative inflation increases the ensemble projections onto weakly-stable and stable modes, it does not entirely accounts for analysis errors on those directions. This motivates the adoption of a complementary inflation strategy to treat errors that lay on the more stable portion of the ensemble. One of the challenges of such an approach is to identify directions which are orthogonal to the leading BLVs in an efficient way while also finding the right balance between inflation within and outside leading BLVs.

4 | HYBRID INFLATION SCHEMES

In the previous section, we have shown that, the use of multiplicative inflation in a sequential DA cycle, leads to maintaining error projections beyond the leading unstable modes. We have also seen that, although very beneficial to a better account of model error, it does not suffice alone.

We now try to enhance the benefits of multiplicative inflation by incorporating perturbations outside of the subspace already spanned by the ensemble via additive inflation (Hamill and Whitaker, 2005). As we shall see, the amount of noise to be introduced via additive covariance inflation can be modulated by limiting its effect outside of the subspace spanned by the ensemble. A similar goal was pursued by Chang et al. (2020) with an hybrid gain DA system in which variational corrections were only applied on directions that are orthogonal to the subspace spanned by the analysis ensemble anomalies. Here we investigate whether separating the portion of ensemble anomalies in the span of the BLVs up to the weakly-stable from the vanishing stable directions could enable the design of more sophisticated inflation schemes, targeting additive perturbations only to directions that are not spanned by the ensemble. We explore hybrid multiplicative-additive inflation schemes whereby multiplicative inflation is applied to the unstable

portion of the spectrum while additive inflation to the remaining part. But how can one decompose the anomalies projections to apply such a hybrid approach? A BLV decomposition along the analysis trajectory offers a natural way to achieve this subspace separation. However, explicit computation of BLVs by traditional methods such as QR-decomposition is too expensive and becomes unfeasible for large scale dynamics such as geophysical systems. Given the alignment of the long-term ensemble anomalies onto the unstable-neutral and weakly-stable subspaces described in the previous section, a real time approximation to split the subspaces affected by the hybrid inflation can be based on the anomalies themselves.

We first decompose the anomaly matrix $\mathbf{A}$ using singular value decomposition (SVD). Under the usual assumption that $N \leq n$, the anomalies matrix $\mathbf{A}$ can be broken down using the reduced singular value decomposition: $\mathbf{A} = \mathbf{U}\mathbf{S}\mathbf{V}^\top$, with $\mathbf{U} \in \mathbf{R}^{n\times N}$, $\mathbf{S} \in \mathbf{R}^{N\times N}$ and $\mathbf{V}^\top \in \mathbf{R}^{N\times N}$. The diagonal matrix $\mathbf{S}$ contains the N singular values of $\mathbf{A}$. As shown in Section 3, $\mathbf{P}^{\mathrm{a}}$ is highly aligned with the neutral-unstable subspace while the remaining variability is associated to (asymptotically) vanishing weakly-stable directions. A similar alignment was found for the filter $\mathbf{P}^{\mathrm{f}}$ matrix. We define $\mathbf{A}^{\mathcal{U}} \in \mathbf{R}^{n\times N}$ as the matrix containing the projections of the anomalies onto the span of the most unstable portion of the BLV spectrum. This matrix will be referred to as unstable anomalies matrix. It is obtained by considering the first s_0 columns (rows) of $\mathbf{U}$ ($\mathbf{V}^\top$) in the reduced singular value decomposition. This is, dropping time dependencies,

$$\mathbf{A}^{\mathcal{U}} = \mathbf{U}^{(:,1:s_0)}\mathbf{S}^{(1:s_0,1:s_0)}{\mathbf{V}^{(:,1:s_0)}}^\top, \tag{7}$$

where the threshold s_0 is defined as the number of singular values that account for a given threshold of its cumulative sum. The threshold is set to 95%. We conducted sensitivity experiments to find that this value is a relatively accurate indicator of the number of BLVs onto which the ensemble anomalies have non-negligible projections over time when using adaptive multiplicative inflation. Indeed when accounting for 95% of cumulative variance, the number of singular values s_0 is on average 22 and 13 for the experiments with and without model errors respectively. These numbers are in agreement with the number of leading BLVs onto which ensemble anomalies have non-negligible projections (cf. Section 3).

Using Eq. 7, we performed an additional idealized experiment in which model error realizations are sampled from $\mathcal{N}(0, \sigma_q \mathbf{\Pi}^{\mathcal{U}}_{\boldsymbol{k}}\mathbf{Q}\mathbf{\Pi}^{\mathcal{U}}_{\boldsymbol{k}})$, where $\mathbf{\Pi}^{\mathcal{U}}_{\boldsymbol{k}} = \mathbf{A}^{\mathcal{U}}_k\mathbf{A}^{\mathcal{U}+}_k$ is a unitary operator and is the orthogonal projector onto the column space of $\mathbf{A}^{\mathcal{U}}_k$, with $\mathbf{A}^{\mathcal{U}+}_k$ being the Moore-Penrose pseudo-inverse of $\mathbf{A}^{\mathcal{U}}_k$. In this case, model error instances are ensured to belong to the span of the ensemble. Not surprisingly, the RMSE is almost identical to the assimilation experiments in which model error instances were projected onto the span of the locally unstable BLVs. The mean angle between ensemble anomalies and BLVs is shown in Fig. 5a (light purple line).

The remaining $(N - s_0)$ columns (rows) of $\mathbf{U}$ ($\mathbf{V}^\top$) are used to define the stable anomalies matrix:

$$\mathbf{A}^{\mathcal{S}} = \mathbf{U}^{(:,s_0+1:N)}\mathbf{S}^{(s_0+1:N,s_0+1:N)}{\mathbf{V}^{(:,s_0+1:N)}}^\top. \tag{8}$$

By definition, matrices $\mathbf{A}^{\mathcal{U}}$ and $\mathbf{A}^{\mathcal{S}}$ are mutually orthogonal $(n \times N)$ matrices of rank s_0 and $(N - s_0)$ respectively, so the anomalies matrix at time t_k can be written as

$$\mathbf{A}_k = \mathbf{A}^{\mathcal{U}}_k + \mathbf{A}^{\mathcal{S}}_k, \tag{9}$$

and,

$$(N-1)\mathbf{P}_k^f = \mathbf{A}_k^{\mathcal{U}}\mathbf{A}_k^{\mathcal{U}^\top} + \mathbf{A}_k^{\mathcal{S}}\mathbf{A}_k^{\mathcal{S}^\top}. \tag{10}$$

Stable and unstable anomalies projections onto BLVs are shown in Fig. 6 using the experimental settings defined in Section 3 for the same model error configurations (*i.e.*, $\sigma_q = 0.0025$ and $\sigma_q = 0.005$). In each case s_0 is dynamically adjusted to account for the corresponding percentage of $\mathbf{P}^{\mathrm{f}}$ total variance and the multiplicative inflation is adaptively adjusted. Anomalies associated to $A^{\mathcal{U}}$ are not only constrained to BLVs associated to asymptotically unstable LLEs, but indeed they span a subspace of higher dimensions. This subspace is increased or decreased based on the level of multiplicative inflation associated to each configuration of model error (see Table 1 for reference). In contrast, $A^{\mathcal{S}}$ anomalies are largely aligned with higher order BLVs. In fact the larger s_0 the higher the order of the BLVs where the residual variance is explained (see how the corresponding yellow lines shift toward right in both panels of Fig. 6). It should be noted that $A^{\mathcal{S}}$ accounts for a tiny portion of the total variance of $\mathbf{P}^{\mathrm{f}}$, representing residual ensemble anomalies that lay mostly outside of the unstable subpsace.

Using the proposed decomposition, it is possible to replicate the span of the locally unstable and weakly stable BLVs, to which one has not usually access in realistic high-dimensional cases due to their prohibitive computational cost. However, this type of decomposition depends on the chosen total variance threshold, which impacts on s_0. As model error increases, the optimal multiplicative inflation needed will also increase. Therefore, it is expected that the proportion of anomalies projecting onto stable BLVs will increase. Consequently, larger values of s_0 are required to properly disentangle anomalies. Moreover, the possible incorporation of additive inflation through random perturbations may have an instantaneous effect similar to the introduction of model errors and will also lead to a shift toward higher values of s_0 for a given variance threshold. These type of feedback processes will drive the need for further threshold adjustments which are outside of the scope of this work.

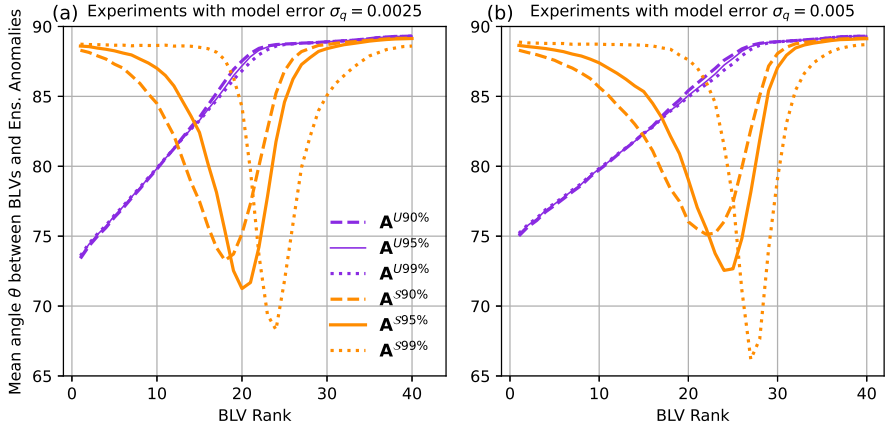

FIGURE 6 Time and ensemble averaged angle θ (degrees) of the dynamically unstable (purple) and stable (orange) portion of ensemble anomalies $\mathbf{A}^U$ (purple) onto the backward Lyapunov vectors for experiments with model errors (a) $\sigma_q = 0.0025$ and (b) $\sigma_q = 0.005$. Multiple thresholds for the amount of total variance in $\mathbf{P}^{\mathrm{f}}$ accounted by unstable anomalies are shown (i.e. 90%, 95%, 99%).

The decomposition in Eq. 10 allows us to design inflation schemes that operate distinctively over the portions of the covariance matrix aligned onto the unstable and stable BLVs respectively. We choose to inflate the unstable anomalies with a multiplicative inflation scheme such that $\mathbf{A}_k'^{\mathcal{U}} = \sqrt{\rho}\mathbf{A}_k^{\mathcal{U}}$. Conversely, for the stable portion of the spectrum, we propose an additive inflation mechanism that attempts to account for errors accumulating on this portion of the spectrum as shown in Fig. 5b (blue line). Additive inflation is thus incorporated on directions that are orthogonal to the leading s_0 anomalies directions but not necessarily limited to the remaining $N-s_0$ anomalies directions, following model error covariance $\mathbf{Q}$. The most unstable directions are properly inflated by the effect of multiplicative inflation alone. We propose two hybrid additive-multiplicative inflation schemes that are the content of the following sections.

4.1 | Hybrid projected stochastic inflation

Additive covariance inflation schemes (*e.g.* Whitaker et al., 2008, Hamill and Whitaker, 2005) consist of drawing random perturbations from a specified error distribution, and adding them to the (prior) forecast ensemble before being updated. Usually these perturbations do not take into account model dynamics and are usually sampled from a full rank covariance matrix. In contrast, we are interested in sampling them from a subspace orthogonal to the unstable BLVs. Using the non-stable anomalies projector defined in the previous section, $\mathbf{\Pi}_k^{\mathcal{U}} = \mathbf{A}^{\mathcal{U}}\mathbf{A}^{\mathcal{U}+}$, random samples can be drawn that are orthogonal to the non-stable modes. The inflated anomalies used for ETKF analysis calculations are then

$$\mathbf{A_k}' = \sqrt{\rho}\mathbf{A}_k^{\mathcal{U}} + \mathbf{A}_k^{\mathcal{S}} + \sqrt{\sigma_q}(\mathbf{I} - \mathbf{\Pi}_k^{\mathcal{U}})\mathbf{Q}^{1/2}\Xi_k, \tag{11}$$

with $\Xi = \{\boldsymbol{\xi}_1, \boldsymbol{\xi}_2, \ldots, \boldsymbol{\xi}_N\}$, and all $\boldsymbol{\xi}_i$ are centered independent random draws from $\mathcal{N}(0, \mathbf{I}_n)$. By construction, the last two terms in Eq. 11 span a subspace orthogonal to the unstable and weakly-stable anomalies subspace spanned by the ensemble. The introduction of stochastic noise not aligned with the unstable anomalies leads to a slightly more uniform eigenspectrum for the covariance matrix. These changes have a direct impact on the value of s_0, which is now increased proportionally with the amplitude of stochastic additive inflation. To account for this, we set s_0 as the number of singular values required to achieve at least 90% of cumulative percentage sum of singular values.

Perturbations associated to non-stable modes are inflated through a multiplicative inflation scheme instead (first term on the r.h.s. of Eq. 11). The adaptive multiplicative inflation scheme of Miyoshi (2011) was extended to this framework in order to scale the inflation coefficient only by taking into account the non-stable portions of the spectrum. Details of this modified adaptive scheme are given in Appendix A.

4.2 | Hybrid projected deterministic inflation

Our second hybrid approach is inspired by the work of Raanes et al. (2015). In this approach the additive inflation acts on the forecast step to account for model errors via a deterministic transformation of the ensemble anomalies. By doing so, it removes the randomness associated to the stochastic sampling step of the additive inflation Hamill and Whitaker (2005). This approach is specifically designed for square-root EnKFs (Tippett et al., 2003). The base implementation, named SQRT-CORE in Raanes et al. (2015), aims to inflate the covariance matrix consistently with the model error covariances according to

$$\mathbf{P}^{\mathrm{f}} = \frac{1}{(N-1)}\mathbf{A}\mathbf{A}^{\top} + \mathbf{A}\mathbf{A}^{+}\mathbf{Q}\mathbf{A}\mathbf{A}^{+}, \tag{12}$$

where temporal dependencies on Eq. (12) were dropped for conciseness. The propoposed formulation ensures that covariance is inflated only in the span of the ensemble anomalies, however only a portion of model error $\mathbf{Q}$ is accounted with this formulation. To satisfy Eq. (12), Raanes et al. (2015) proposed the following (symmetric) square root formulation for the anomalies,

$$\mathbf{A}' = \mathbf{A}\mathbf{T} = \mathbf{A}[\mathbf{I}_N + (N-1)\mathbf{A}^{+}\mathbf{Q}(\mathbf{A}^{+})^{\top}]^{1/2}. \tag{13}$$

Based on the above, we propose an hybrid inflation scheme similar in the spirit of the one in Section 4.1 but that avoids the stochastic term. This second approach, named *hybrid projected deterministic inflation*, consists in confining the deterministic inflation scheme SQRT-CORE from Raanes et al. (2015) to the span of the stable anomalies. This is,

$$\mathbf{A}'^{\mathcal{S}} = \mathbf{A}^{\mathcal{S}}[\mathbf{I}_N + \sigma_q(N-1)\mathbf{A}^{\mathcal{S}^{+}}\mathbf{Q}(\mathbf{A}^{\mathcal{S}^{+}})^{\top}]^{1/2}. \tag{14}$$

The inflated covariances can be reconstructed as in Eq. (10), since again inflated anomalies $\mathbf{A}'^{\mathcal{S}}$ belong to the span of $\mathbf{A}^{\mathcal{S}}$ and are thus orthogonal to $\mathbf{A}^{\mathcal{U}}$. The threshold s_0 is defined using the same criterion as in the projected stochastic inflation scheme of the previous section. For anomalies aligned with non-stable modes an adaptive multiplicative covariance inflation scheme is used. The resulting inflated anomalies are then

$$\mathbf{A_k}' = \sqrt{\rho}\mathbf{A}_k^{\mathcal{U}} + \mathbf{A}'^{\mathcal{S}}_k. \tag{15}$$

We emphasize that the hybrid projected deterministic inflation in Eqs. (14)–(15) differs from the hybrid projected stochastic inflation of Section 4.1 not only due to its deterministic nature, but most importantly due to additive inflation being constrained to the subspace of stable anomalies spanned by the ensemble. It also distinguishes from standard multiplicative inflation by incorporating perturbations that are proportional to $\mathbf{Q}$ and are completely aligned with the most stable directions of the ensemble.

4.3 | Comparing the hybrid inflation schemes

The proposed hybrid inflation schemes are compared numerically under the model configuration of Section 3 with $\sigma_q = 0.005$. The hybrid schemes are compared against two baselines: the adaptive multiplicative inflation scheme from Miyoshi (2011) and the additive inflation scheme in which forecasts are inflated additively with random perturbations sampled from $\mathcal{N}(0, \mathbf{Q})$. For a more fair comparison, random perturbations from the additive inflation scheme are scaled by a factor of $\gamma = 1.18$, this value was obtained from an exhaustive search to optimize RMSE.

In hybrid schemes, the multiplicative inflation applied to the unstable portion of anomalies is estimated adaptively at each assimilation cycle using the approach in Miyoshi (2011). We also include the results using the *SQRT-DEP* scheme. This is an extension of the additive inflation SQRT- CORE scheme proposed by Raanes et al. (2015) that

accounts for stochastic perturbations sampled from outside the ensemble subspace plus a stochastic correction for potential residual effects within the ensemble subspace (see Raanes et al., 2015, their Section 6). The RMSE, the additive inflation scaling factor, and the mean optimal multiplicative inflation factor for each scheme are given in Table 2. The RMSE values achieved using the different schemes are very similar, although the hybrid projection deterministic scheme performs slightly better than its stochastic counterpart. This suggests that mitigating sampling errors in the additive inflation term is beneficial. Along this line, we see that compared to SQRT-DEP, the hybrid stochastic schemes are not able to achieve the same level of RMSE, emphasizing the impact of sampling errors associated to stochastic additive inflation schemes.

The hybrid schemes have an average value of $s_0 = 22$ and $s_0 = 24$ for the stochastic and deterministic cases respectively. This implies that a larger portion of the anomalies space is treated via multiplicative inflation in the deterministic version. The projection of ensemble anomalies onto BLVs is shown in Fig. 7a. The hybrid schemes show a very similar projection onto BLVs of rank $r < 22$, indicating that the differences in the value of s_0 for the hybrid schemes may not play a dominant role. For the multiplicative scheme, the projection onto higher order BLVs is progressively reduced, and the reduction ratio remains quite uniform. In contrast, the introduction of inflation in directions that are orthogonal to the unstable BLVs helps to retain more effectively perturbations that align with BLVs of rank $r > 20$ onto the subspace spanned by unstable and weakly stable BLVs. The hybrid projected deterministic schemes incorporates multiplicative inflation only in the subspace spanned by the ensemble, hence the anomalies covariance matrix cannot span the full subspace spanned by the BLVs (see red line in Fig. 7a). On the other hand, the non-multiplicative inflation portion in the hybrid stochastic inflation scheme is also projected onto the part of the ensemble which is not necessarily aligned with the unstable directions, while consistently sampling from $\mathbf{Q}$. The alignment of anomalies with BLVs for this scheme holds a large resemblance with the SQRT-DEP method. This is related to the fact that both schemes not only inflate ensemble anomalies, but they also combine them with random noise sampled from a subspace orthogonal to the ensemble subspace. As a comparison, the additive inflation scheme leads to covariances with about the same degree of projection onto BLVs. However, this type of projection analysis ignores the contribution of anomalies which are orthogonal to BLVs subspace, which may be responsible for its poorer performance in terms of RMSE.

Analysis errors projected onto the BLVs do not differ significantly among the hybrids and SQRT-DEP schemes. All schemes that explicitly inflate directions outside the leading unstable and weakly stable BLVs reduce errors by projecting on higher order BLVs when compared to multiplicative inflation alone.

TABLE 2 RMSE for several inflation schemes

	RMSE	Unstable inflation factor	Stable inflation factor
Multiplicative inflation	0.0163	α =1.18	α =1.18
Additive inflation	0.0177	γ =1.18	γ =1.18
Hybrid proj. stochastic inflation	0.0160	α =1.13	α =1.00
Hybrid proj. deterministic inflation	0.0152	α =1.11	α =1.00
SQRT-DEP	0.0151	α =1.00	α =1.00

The proposed experimental framework is intentionally characterized by a strong observational constraint. We performed an additional set of experiments with half of the observations, namely we observe only every other variable.

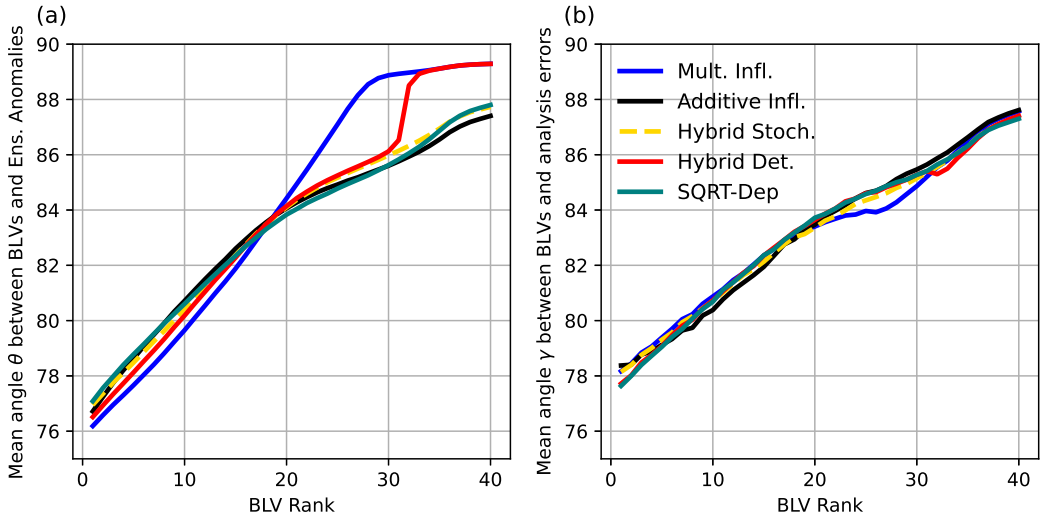

FIGURE 7 (a) Time and ensemble averaged angle θ (degrees) of the ensemble anomalies projected onto the backward Lyapunov vectors (BLVs) for the multiplicative inflation scheme (blue), standard additive inflation scheme (black), hybrid projected stochastic inflation (yellow), hybrid projected deterministic inflation (red) and SQRT-DEP (green). (b) Time and ensemble averaged angle γ (degrees) of the analysis errors projected onto the backward Lyapunov vectors (BLVs) for the same assimilation configurations

Observations frequency remains the same as in Section 3. this case. The reduced density of observations alleviates the need of multiplicative inflation across all of the experiments with adaptive inflation (*cf.* Table 3). The analysis RMSE improvement using the hybrid schemes was around 10% with respect to multiplicative inflation, which is very close to the results obtained in the fully observed case. While the ensemble anomalies projection shown in Fig. 8 gains several features from the previous experiment, it should be noticed that the angle of projection onto the stable modes is smaller in this case. For the case with only multiplicative inflation, the ensemble anomalies span a reduced subspace of the BLV spectrum. This may indicate that the ensemble is constrained to a reduced subspace where model dynamics play a more dominant role than model errors.

TABLE 3 RMSE for several inflation schemes - Reduced observations network

	RMSE	Unstable inflation factor	Stable inflation factor
Multiplicative inflation	0.0221	α =1.14	α =1.14
Hybrid proj. stochastic inflation	0.0217	α =1.09	α =1.00
Hybrid proj. deterministic inflation	0.0202	α =1.07	α =1.00
SQRT-DEP	0.0201	α =1.00	α =1.00

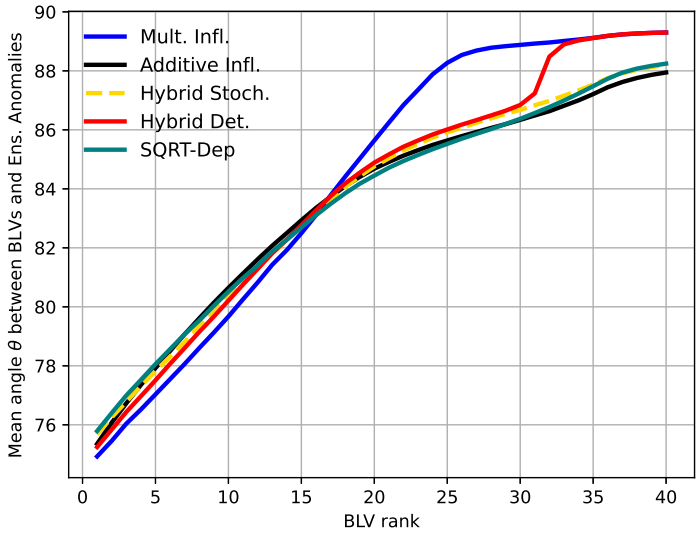

FIGURE 8 Same as in REF but assuming observations are only available at every other grid point.

5 | DISCUSSIONS

In this work, the combined dynamical effects of model error and covariance inflation on ensemble Kalman filtering have been examined. We focused on deterministic EnKF and used the ETKF as prototypical. Our primary interest was on the geometrical properties of the ensemble-based analysis error covariance, in particular on how they project onto the natural unstable modes of the dynamics.

Previous works have investigated the relation between the span of the error covariance and the unstable-neutral subspace in perfect and in the model error scenario. Those results are reviewed in Carrassi et al. (2022). However, the impact of model error and inflation on the geometry of EnKF error covariance had not yet been studied.

The main findings of the previous works can be summarised as follow. In the absence of model error, the long-term rank and span of the ensemble-based covariances respectively converges to the number of unstable and neutral Lyapunov exponents and projects on the subspace spanned by the unstable-neutral backward Lyapunov vectors (BLVs). In the presence of model error, Grudzien et al. (2018b) showed that weakly-stable BLVs play a little, yet not negligible, role in shaping the subspace where errors are confined, and weakly-stable modes must be considered in the reduced-rank filter design. Following on from the work of Grudzien et al. (2018b) here we studied the effects of model error and of multiplicative and additive covariance inflation over ensemble dynamics.

First, we demonstrated that, differently from what one would expect, the use of multiplicative inflation alone is enough to retain anomalies in the span of weakly stable BLVs, regardless of the presence of model error. The number of weakly-stable BLVs that support the Kalman filter analysis covariance matrix seems to be dynamically adjustable via multiplicative inflation. This mechanism may explain the success of multiplicative inflation schemes in accounting for model errors, in line with the findings in Grudzien et al. (2018b) for the extended Kalman filter. The latter in fact

typically lay everywhere and thus also outside of the unstable subspace that supports the ensemble. The increase of subspace via multiplicative inflation is a purely dynamical mechanism, determined by the sequential nature of the EnKF. In fact, inflation repeatedly counteract the damping of stable modes. Even when nonlinear dynamics are expected to drive perturbations towards the leading unstable modes, the successive application of multiplicative inflation and model forecasts will prevent the banishment of stable modes.

Nevertheless, multiplicative inflation alone is not enough to reproduce the alignment of analysis errors with the BLVs which, in the presence of model errors, show a stronger projection onto the stable part of the BLV spectrum. This motivates the combination of multiplicative inflation with additive inflation approaches which can increase the projection of the ensemble perturbations onto the stable part of the BLV spectrum.

Assuming that the unstable and leading weakly-stable modes can be represented by means of a properly tuned multiplicative inflation scheme, we propose two methods that attempt to represent and incorporate model errors associated to the remaining asymptotically stable modes. In this way, we divide the treatment of sampling errors on the unstable modes from the need for representing the model errors effects on the stable subspace. The proposed methods are based on a singular value decomposition of the forecast anomalies to isolate the components associated to the more stable modes. The proposed methods aid to understand the impact of additive inflation on the presence of model error. An alternative approach to exploit the subspace orthogonal to the ensemble space through a variational correction was proposed by Chang et al. (2020) in the scope of hybrid-gain DA.

Our results suggest that errors are expected to have a more uniform projection onto the BLVs as model error increases. We have not included alternative model error representations such as parametric errors (Nicolis et al., 2009). By changing parameters, we could end up on scenario where dynamics and its associated unstable subspace may differ between model and nature runs. This work uses controlled experiments in which covariance matrices $\mathbf{Q}$ and $\mathbf{R}$ are assumed to be known and there are enough observations to ensure a nearly linear evolution of errors. Future work should evaluate how the results could be extended in experiments with more realistic settings. In particular, it could be interesting to evaluate the performance of the hybrid schemes with an increased level of nonlinearity. In that scenario, the representation of errors outside of the unstable modes may have a critical role. It is possible, nevertheless, that multiplicative inflation alone is enough to align the filter towards the subspace spanned by a suitable number of BLVs in that case too.

6 | APPENDIX A - ADAPTIVE MULTIPLICATIVE INFLATION FOR UNSTABLE SUBSPACE

The adaptive multiplicative covariance inflation scheme used in this work is outlined in Miyoshi (2011). This scheme exploits one of the diagnostic relationships described by Desroziers et al. (2005), namely

$$\langle \mathbf{d}\mathbf{d}^{\mathsf{T}} \rangle = \mathbf{H}\mathbf{B}\mathbf{H}^{\mathsf{T}} + \mathbf{R}, \tag{16}$$

where $\mathbf{d} = \mathbf{y} - \mathbf{H}\mathbf{x}^{\mathrm{b}}$ are the observation minus background innovations and $\mathbf{B}$ is the background covariance matrix. This relationship is valid as long as the observation and background errors are perfectly specified. For the ensemble Kalman filter, the equation can be approximated by incorporating an inflation factor to the ensemble derived forecast errors covariance matrix.

$$\langle \mathbf{d}\mathbf{d}^{\mathsf{T}} \rangle = \alpha \mathbf{H}\mathbf{P}^{\mathsf{f}}\mathbf{H}^{\mathsf{T}} + \mathbf{R}, \tag{17}$$

Based on diagonals terms, the optimal instantaneous coefficient can be inferred as

$$\alpha = \frac{\langle \mathbf{d}\mathbf{d}^{\mathsf{T}} \rangle - \mathrm{tr}(\mathbf{R})}{\mathrm{tr}(\mathbf{H}\mathbf{P}^{\mathsf{f}}\mathbf{H}^{\mathsf{T}})}, \tag{18}$$

To adjust the adaptive multiplicative inflation factor to the unstable subspace we modify Eq. 18 in order to bound it to the unstable subspace

$$\alpha^{\mathcal{U}} = \frac{\langle \mathbf{d}\mathbf{d}^{\mathsf{T}} \rangle - \mathrm{tr}(\mathbf{H}\mathbf{A}^{\mathcal{S}}\mathbf{A}^{\mathcal{S}\mathsf{T}}\mathbf{H}^{\mathsf{T}})/(\mathrm{N}-1) - \mathrm{tr}(\mathbf{R})}{\mathrm{tr}(\mathbf{H}\mathbf{A}^{\mathcal{U}}\mathbf{A}^{\mathcal{U}\mathsf{T}}\mathbf{H}^{\mathsf{T}})/(\mathrm{N}-1)}, \tag{19}$$

Instantaneous estimations of inflation factor should however take into account uncertainties associated to sampling and unsuitable definition of $\mathbf{R}$ -the latter is not an issue in our synthetic setup. For this reason, the inflation factor is updated using a scalar Kalman filter ensuring also a smooth convergence towards an optimal value. A detailed discussion of parameter update process is given by Li et al. (2009) and also by Miyoshi (2011).

acknowledgements

We thank the two anonymous reviewers for their insightful comments that have helped to improve much the first version of the manuscript. This work was partially financed by Agencia Nacional de Promoción Científica y Tecnologica, PICT: 2033/2017 and University of Buenos Aires 20020170100504BA grants. Alberto Carrassi acknowledges the support of the UK National Centre for Earth Observation (grant no. NCEO02004). Alberto Carrassi is also supported by the project SASIP funded by Schmidt Futures – a philanthropic initiative that seeks to improve societal outcomes through the development of emerging science and technologies

references

Anderson, J. (2009) Spatially and temporally varying adaptive covariance inflation for ensemble filters. *Tellus A: Dynamic Meteorology and Oceanography*, **61**, 72–83.

Anderson, J. L. and Anderson, S. L. (1999) A monte carlo implementation of the nonlinear filtering problem to produce ensemble assimilations and forecasts. *Monthly Weather Review*, **127**, 2741–2758.

Bishop, G., Welch, G. et al. (2001) An introduction to the kalman filter. *Proc of SIGGRAPH, Course*, **8**, 41.

Bocquet, M. and Carrassi, A. (2017) Four-dimensional ensemble variational data assimilation and the unstable subspace. *Tellus A: Dynamic Meteorology and Oceanography*, **69**, 1304504.

Bocquet, M., Gurumoorthy, K. S., Apte, A., Carrassi, A., Grudzien, C. and Jones, C. K. (2017) Degenerate kalman filter error covariances and their convergence onto the unstable subspace. *SIAM/ASA Journal on Uncertainty Quantification*, **5**, 304–333.

Bocquet, M., Raanes, P. N. and Hannart, A. (2015) Expanding the validity of the ensemble kalman filter without the intrinsic need for inflation. *Nonlinear Processes in Geophysics*, **22**, 645–662.

Carrassi, A., Bocquet, M., Demaeyer, J., Grudzien, C., Raanes, P. and Vannitsem, S. (2022) *Data Assimilation for Chaotic Dynamics*, 1–42. Cham: Springer International Publishing. URL: https://doi.org/10.1007/978-3-030-77722-7_1.

Chang, C.-C., Penny, S. G. and Yang, S.-C. (2020) Hybrid gain data assimilation using variational corrections in the subspace orthogonal to the ensemble. *Monthly Weather Review*, **148**, 2331–2350.

Dee, D. P. (1995) On-line estimation of error covariance parameters for atmospheric data assimilation. *Monthly weather review*, **123**, 1128–1145.

Desroziers, G., Berre, L., Chapnik, B. and Poli, P. (2005) Diagnosis of observation, background and analysis-error statistics in observation space. *Quarterly Journal of the Royal Meteorological Society: A journal of the atmospheric sciences, applied meteorology and physical oceanography*, **131**, 3385–3396.

El Gharamti, M. (2018) Enhanced adaptive inflation algorithm for ensemble filters. *Monthly Weather Review*, **146**, 623–640.

El Gharamti, M., Raeder, K., Anderson, J. and Wang, X. (2019) Comparing adaptive prior and posterior inflation for ensemble filters using an atmospheric general circulation model. *Monthly Weather Review*, **147**, 2535–2553.

Evensen, G. et al. (2009) *Data assimilation: the ensemble Kalman filter*, vol. 2. Springer.

Grudzien, C., Carrassi, A. and Bocquet, M. (2018a) Asymptotic forecast uncertainty and the unstable subspace in the presence of additive model error. *SIAM/ASA Journal on Uncertainty Quantification*, **6**, 1335–1363.

— (2018b) Chaotic dynamics and the role of covariance inflation for reduced rank kalman filters with model error. *Nonlinear Processes in Geophysics*, **25**, 633–648.

Gurumoorthy, K. S., Grudzien, C., Apte, A., Carrassi, A. and Jones, C. K. (2017) Rank deficiency of kalman error covariance matrices in linear time-varying system with deterministic evolution. *SIAM Journal on Control and Optimization*, **55**, 741–759.

Hamill, T. M. and Whitaker, J. S. (2005) Accounting for the error due to unresolved scales in ensemble data assimilation: A comparison of different approaches. *Monthly weather review*, **133**, 3132–3147.

Hunt, B. R., Kostelich, E. J. and Szunyogh, I. (2007) Efficient data assimilation for spatiotemporal chaos: A local ensemble transform kalman filter. *Physica D: Nonlinear Phenomena*, **230**, 112–126.

Legras, B. and Vautard, R. (1996) A guide to liapunov vectors. In *Proceedings 1995 ECMWF seminar on predictability*, vol. 1, 143–156. Citeseer.

Li, H., Kalnay, E. and Miyoshi, T. (2009) Simultaneous estimation of covariance inflation and observation errors within an ensemble kalman filter. *Quarterly Journal of the Royal Meteorological Society: A journal of the atmospheric sciences, applied meteorology and physical oceanography*, **135**, 523–533.

Lorenz, E. N. (1996) Predictability: A problem partly solved. In *Proc. Seminar on predictability*, vol. 1.

Lorenz, E. N. and Emanuel, K. A. (1998) Optimal sites for supplementary weather observations: Simulation with a small model. *Journal of the Atmospheric Sciences*, **55**, 399–414.

Miyoshi, T. (2011) The gaussian approach to adaptive covariance inflation and its implementation with the local ensemble transform kalman filter. *Monthly Weather Review*, **139**, 1519–1535.

Nicolis, C., Perdigao, R. A. and Vannitsem, S. (2009) Dynamics of prediction errors under the combined effect of initial condition and model errors. *Journal of the atmospheric sciences*, **66**, 766–778.

Palatella, L., Carrassi, A. and Trevisan, A. (2013) Lyapunov vectors and assimilation in the unstable subspace: theory and applications. *Journal of Physics A: Mathematical and Theoretical*, **46**, 254020.

Pulido, M., Tandeo, P., Bocquet, M., Carrassi, A. and Lucini, M. (2018) Stochastic parameterization identification using ensemble kalman filtering combined with maximum likelihood methods. *Tellus A: Dynamic Meteorology and Oceanography*, **70**, 1–17.

Raanes, P. N., Bocquet, M. and Carrassi, A. (2019) Adaptive covariance inflation in the ensemble kalman filter by gaussian scale mixtures. *Quarterly Journal of the Royal Meteorological Society*, **145**, 53–75.

Raanes, P. N., Carrassi, A. and Bertino, L. (2015) Extending the square root method to account for additive forecast noise in ensemble methods. *Monthly Weather Review*, **143**, 3857–3873.

Tandeo, P., Ailliot, P., Bocquet, M., Carrassi, A., Miyoshi, T., Pulido, M. and Zhen, Y. (2020) A review of innovation-based methods to jointly estimate model and observation error covariance matrices in ensemble data assimilation. *Monthly Weather Review*, **148**, 3973–3994.

Tippett, M. K., Anderson, J. L., Bishop, C. H., Hamill, T. M. and Whitaker, J. S. (2003) Ensemble square root filters. *Monthly Weather Review*, **131**, 1485–1490.

Tondeur, M., Carrassi, A., Vannitsem, S. and Bocquet, M. (2020) On temporal scale separation in coupled data assimilation with the ensemble kalman filter. *Journal of Statistical Physics*, **179**, 1161–1185.

Whitaker, J. S. and Hamill, T. M. (2012) Evaluating methods to account for system errors in ensemble data assimilation. *Monthly Weather Review*, **140**, 3078–3089.

Whitaker, J. S., Hamill, T. M., Wei, X., Song, Y. and Toth, Z. (2008) Ensemble data assimilation with the ncep global forecast system. *Monthly Weather Review*, **136**, 463–482.

Zheng, X. (2009) An adaptive estimation of forecast error covariance parameters for kalman filtering data assimilation. *Advances in Atmospheric Sciences*, **26**, 154–160.